

DOI: 10.1002/chem.200601855

DNA Binding by a New Metallointercalator that Contains a Proflavine Group Bearing a Hanging Chelating Unit

Carla Bazzicalupi,^[a] Andrea Bencini,^[a] Antonio Bianchi,^{*[a]} Tarita Biver,^[b] Alessia Boggioni,^[b] Sara Bonacchi,^[a] Andrea Danesi,^[a] Claudia Giorgi,^[a] Paola Gratteri,^[c] Antonio Marchal Ingraín,^[d] Fernando Secco,^{*[b]} Claudia Sissi,^[e] Barbara Valtancoli,^[a] and Marcella Venturini^[b]

Abstract: The new bifunctional molecule 3,6-diamine-9-[6,6-bis(2-aminoethyl)-1,6-diaminohexyl]acridine (**D**), which is characterised by both an aromatic moiety and a separate metal-complexing polyamine centre, has been synthesised. The characteristics of **D** and its Zn^{II} complex ([Zn**D**]) (protonation and metal-complexing constants, optical properties and self-aggregation phenomena) have been analysed by means of NMR spectroscopy, potentiometric, spectrophotometric and spectrofluorimetric techniques. The equilibria and kinetics of the binding process of **D** and [Zn**D**] to calf thymus DNA

have been investigated at $I=0.11\text{ M}$ (NaCl) and 298.1 K by using spectroscopic methods and the stopped-flow technique. Static measurements show biphasic behaviour for both **D**-DNA and [Zn**D**]-DNA systems; this reveals the occurrence of two different binding processes depending on the polymer-to-dye molar ratio (**P/D**). The binding mode that occurs at low **P/D** values is interpreted in terms of external binding

with a notable contribution from the polyamine residue. The binding mode at high **P/D** values corresponds to intercalation of the proflavine residue. Stopped-flow, circular dichroism and supercoiled-DNA unwinding experiments corroborate the proposed mechanism. Molecular-modelling studies support the intercalative process and evidence the influence of NH⁺...O interactions between the protonated acridine nitrogen atom and the oxygen atoms of the polyanion; these interactions play a key role in determining the conformation of DNA adducts.

Keywords: DNA • kinetics • molecular modelling • proflavine derivatives • zinc

Introduction

Recent developments in biochemistry concern the design of new molecules that are able to bind and react with DNA,

and the properties of which as drugs need to be tested. These new probes can provide a better understanding of the activity of many drugs and anticancer agents, and can be of help in developing new diagnostic tools.


[a] Dr. C. Bazzicalupi, Prof. A. Bencini, Prof. A. Bianchi, S. Bonacchi, Dr. A. Danesi, Dr. C. Giorgi, Prof. B. Valtancoli
Dipartimento di Chimica, Università di Firenze
Via della Lastruccia 3, 50019, Sesto Fiorentino (Italy)
Fax: (+39)055-4573-364
E-mail: antonio.bianchi@unifi.it

[b] Dr. T. Biver, A. Boggioni, Prof. F. Secco, Prof. M. Venturini
Dipartimento di Chimica e Chimica Industriale
Università di Pisa
Via Risorgimento 35, 56126, Pisa (Italy)
Fax: (+39)050-2219-260
E-mail: ferdi@dcci.unipi.it

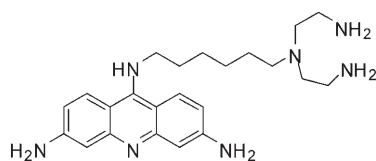
[c] Prof. P. Gratteri
Dipartimento di Scienze Farmaceutiche
Università di Firenze
Via Ugo Schiff 6, 50019 Sesto Fiorentino (Italy)

[d] Prof. A. M. Ingraín
Departamento de Química Inorgánica y Orgánica
Universidad de Jaén
Campus Universitario "Las Lagunillas", 23071-Jaén (Spain)

[e] Dr. C. Sissi
Dipartimento di Scienze Farmaceutiche
Università di Padova
Via Marzolo 5, 35100 Padova (Italy)

 Supporting information for this article is available on the WWW under <http://www.chemeurj.org/> or from the author.

Actually, the activity of many anticancer, antimalarial and antibacterial agents, and that of aromatic carcinogens finds its origin in intercalative interactions.^[1–3] Acridines are a special class of compounds, not only because of their wide use in the pharmaceutical and dye industries, but also due to their interesting chemical and physical properties.^[4,5] They were the first chromophores the noncovalent interactions of which with DNA were extensively studied by exploiting their intense fluorescence, and their binding to double strands is almost universally interpreted according to intercalation.^[6–9] Numerous studies have shown that the intercalative process is much more complex than was previously thought, and it depends on the intercalating molecule's structure.^[10] In this context, bifunctional molecules that bear both an aromatic moiety and a separate metal-complexing centre appear to be of particular interest.^[11–13] The aromatic residue provides an anchor for the molecule on the polymer chain by intercalation, whereas the metal centre might intercalate as well, or it might interact with the polymeric backbone thereby exerting its function.^[14] Barton and co-workers^[15] have synthesised special metallointercalators with diverse functions, from luminescent probes for DNA^[16] to structural probes for RNA.^[17] Other complexes have been designed to be able to recognise specific sites on DNA as base pair mismatches.^[18] Moreover, metallointercalators that are able to promote the cleavage of the phosphodiester bond at a selected point of the chain length have been prepared. Platinum(II) complexes that have been appended to an aromatic residue are other special metal intercalators. Their possible anticancer activity has made them attractive synthetic targets.^[10,19,20] The intercalative binding of these complexes to nucleic acids constitute a prerequisite for the consequent slow attack of Pt^{II} on the base nitrogen atom.^[21,22] On the basis of the above-mentioned arguments, we found it interesting to synthesise a new fluorescent metallointercalator and to investigate its interaction with double-stranded calf thymus DNA. This molecule, 3,6-diamine-9-[6,6-bis(2-aminoethyl)-1,6-diaminohexyl]acridine, from now on denoted as **D** (dye) is characterised by a proflavine unit with a diethylenetriamine moiety that is able to chelate metal ions. A novel structural aspect of **D** is that the metal-binding site is linked to the C9 position of the acridine group instead of the N10 position, as is the case in similar metallointercalators.^[21] Because the N10 atom of **D** is expected to be protonated at physiological pH in both the metal-free ligand and its metal complexes, we found it interesting to analyse the effect of a positively charged N10 ammonium group on the DNA-binding process. Actually, this ammonium group might be able to influence the interaction



with DNA through the formation of electrostatic and hydrogen-bond interactions with oxygen atoms of the polyanion.

Accordingly, the metal-complex-forming ability of **D** and the thermodynamic and kinetic features of the interaction of **D** and its Zn^{II} complex with DNA have been investigated.

Results

Ligand protonation and Zn^{II} complexation: It is known that acridine derivatives give rise to self-aggregation in aqueous solution with the formation of dimers, or larger oligomeric species at higher concentrations.^[21,23–28] Because the aggregation process can interfere with all other equilibria, the ability of **D** and its Zn^{II} complex to form aggregates was investigated first.

The ¹H NMR spectra in D₂O that were recorded at different pH values and with **D** concentrations greater than 1 × 10^{−3} M showed that in alkaline solutions (pH > 8.5), all resonances are split (Figure 1). This second set of signals reflects the formation of a second equilibrium species that has the same symmetry as the parent one, and the interconversion of which is slow on the NMR timescale. ¹H NMR measurements performed with different ligand concentrations (0.01–0.001 M) and at different temperatures (298–328 K) showed that the abundance of the new species increases with increasing ligand concentration and decreases with increasing temperature, while an opposite trend was found for the other species. These data are in agreement with a dimeric new species that is in equilibrium with monomeric **D**. Molecules of **D** associate with one another and form π-stacking interactions between the heteroaromatic units; this is denoted by the significant upfield shift that is experienced by the acridine protons ($\delta_{H1} - \delta_{H1'} = 0.096$ ppm, $\delta_{H2} - \delta_{H2'} = 0.046$ ppm, $\delta_{H3} - \delta_{H3'} = 0.042$ ppm, pH 10, Figure 1). Furthermore the interconversion between the two species is reversible with respect to changes in pH, concentration and temperature.

To support the ¹H NMR information, we recorded UV/vis absorption spectra of **D** in aqueous solution (pH 10.5) in the concentration range of 1 × 10^{−6}–1 × 10^{−4} M; this showed that no self-association effects were observed under similar dilution conditions.

After taking these results into account, the proton-transfer reactions in aqueous solution were studied with a low dye concentration of [**D**] = 5 × 10^{−4} M to avoid the formation of aggregates. Actually, attempts to determine the stoichiometry and stability constants of such aggregates were made by working at higher ligand concentrations, but no results were obtained at an acceptable level of confidence. The protonation constants that were determined by means of potentiometric titrations are reported in Table 1. In the pH range investigated (pH 2.5–10.5), **D** behaves as a tetraprotic base, in spite of the high number of nitrogen atoms that could, in principle, undergo protonation.

To establish which nitrogen atom is protonated in each protonation stage, we recorded the ¹H NMR spectra of **D** at

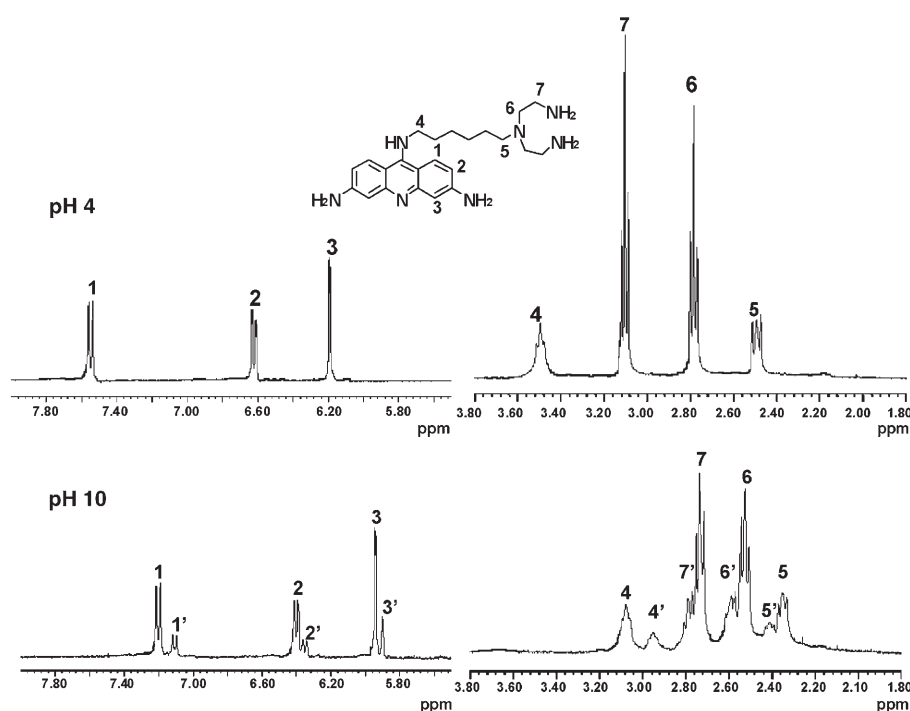


Figure 1. ^1H NMR spectra of **D** (1×10^{-2} M) at pH 4 and pH 10. Primed labels refer to dimeric species.

Table 1. Logarithms of ligand **D** protonation and Zn^{II} complexation constants determined in 0.1 M NMe_4Cl at 298.1 ± 0.1 K.

	log <i>K</i>
$\text{D} + \text{H}^+ \rightleftharpoons [\text{HD}]^+$	10.21(2) ^[a]
$[\text{HD}]^+ + \text{H}^+ \rightleftharpoons [\text{H}_2\text{D}]^{2+}$	9.20(2)
$[\text{H}_2\text{D}]^{2+} + \text{H}^+ \rightleftharpoons [\text{H}_3\text{D}]^{3+}$	8.21(1)
$[\text{H}_3\text{D}]^{3+} + \text{H}^+ \rightleftharpoons [\text{H}_4\text{D}]^{4+}$	2.81(1)
$\text{D} + \text{Zn}^{2+} \rightleftharpoons [\text{ZnD}]^{2+}$	13.59 (8)
$[\text{ZnD}]^{2+} + 2\text{H}^+ \rightleftharpoons [\text{ZnH}_2\text{D}]^{4+}$	13.94 (6)
$[\text{ZnD}]^{2+} + \text{OH}^- \rightleftharpoons [\text{ZnD}(\text{OH})]^+$	3.70 (9)
$2[\text{ZnD}]^{2+} \rightleftharpoons [\text{Zn}_2\text{D}_2]^{4+}$	2.60 (7)
$[\text{Zn}_2\text{D}_2]^{4+} + \text{H}^+ \rightleftharpoons [\text{Zn}_2\text{HD}_2]^{5+}$	7.77 (9)

[a] Values in parentheses are standard deviations on the last significant figure

different pH values. The pH dependence of the ^1H NMR signals (Supporting Information, Figure S1) showed that the first two protonation steps ($\log K = 10.21, 9.20$) take place on the primary nitrogen atoms of the diethylenetriamine group, while the third ($\log K = 8.21$) and the fourth ($\log K = 2.81$) protonations involve the acridine nitrogen atom and the tertiary nitrogen atom of the diethylenetriamine group, respectively, according to the Scheme 1. Such protonation behaviour is in agreement with the greater basicity of aliphatic amines compared to aromatic ones, and with the general behaviour of aminoacridine.^[29,30]

The involvement of the acridine nitrogen atom in the third protonation step was confirmed by the absorption and fluorescence emission spectra that were recorded at different pH values (Supporting Information, Figure S2).

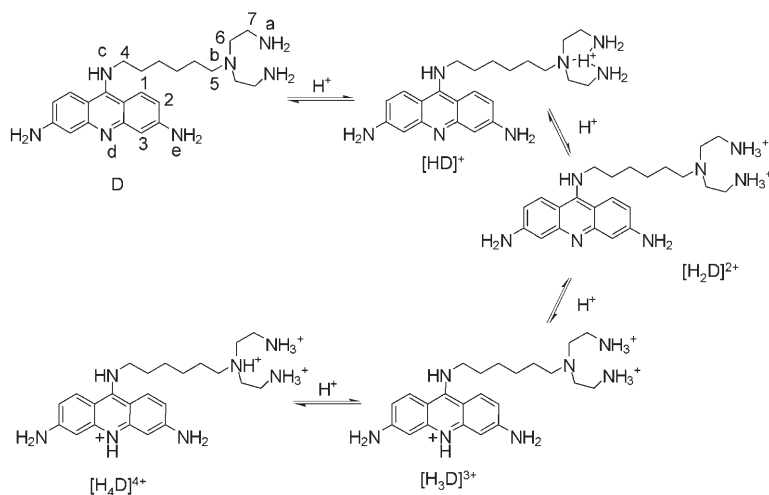
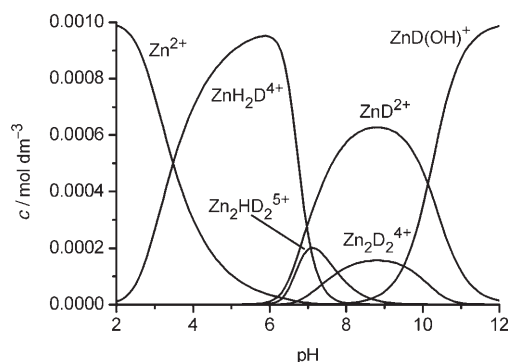
Prior to complexation studies, the possible self-association of complex species was investigated by ^1H NMR measurements in solutions of Zn^{II} and **D** in a 1:1 molar ratio. Although in this case due to broadening of the signals of the aliphatic protons that was caused by coordination of Zn^{II} to the diethylenetriamine moiety the spectra were not well resolved, a splitting of aromatic ^1H signals with the formation of a new set of upfield-shifted resonances (Supporting Information, Figure S3), similar to that observed for the metal-free ligand, revealed the presence of a new complex species at pH values greater than 6, and at a complex concentrations of 5×10^{-4} M or higher. The abundance of this species in solution increases with complex concentration and decreases

with increasing temperature according to an equilibrium between monomeric and π -stacked dimeric species.

Speciation of all complexes was performed by means of potentiometric titrations, and it confirmed the dimeric nature of such species. Table 1 lists the equilibrium constants of all complexes. As shown by the distribution diagram reported in Figure 2, which was calculated for millimolar concentrations of Zn^{II} and **D**, the two dimeric complexes ($[\text{Zn}_2\text{D}_2]^{4+}$, $[\text{Zn}_2\text{HD}_2]^{5+}$) are minor species under these experimental conditions, while the $[\text{ZnD}]^{2+}$ complex and its protonated and hydroxylated forms ($[\text{ZnH}_2\text{D}]^{4+}$, $[\text{ZnD}(\text{OH})]^+$) prevail over all of the pH range. The dimeric species disappear at complex concentrations lower than 1×10^{-4} M, and they become predominant as the concentration is increased. The absence of aggregates under similar dilution conditions was confirmed by the UV/vis absorption spectra of **D**, which was recorded in the concentration range 1×10^{-6} – 1×10^{-4} M.

DNA-binding equilibria: On the basis of the previous results, appropriate concentrations of dyes (1×10^{-5} M) and pH (pH 7 for **D**, pH 8 for $[\text{ZnD}]$) were selected to ensure the absence of dye aggregates in the solutions that were used to study the interaction of **D** and its Zn^{II} complex with DNA. The interaction is revealed by changes in the fluorescence spectra that occur when increasing amounts of DNA are added to a dye solution.

A fluorescence emission study was performed with the metal-free ligand at pH 7, in which $[\text{H}_3\text{D}]^{3+}$ is almost the unique species in solution. This showed a sharp decrease of the emission intensity upon the early additions of DNA to

Scheme 1. Protonation pattern of **D**.Figure 2. Distribution diagram of the Zn^{II} complexes that are formed by **D** as a function of pH ($C_{\text{Zn(II)}} = C_{\text{D}} = 1 \times 10^{-3}$ M). $I = 0.10$ M (NMe₄Cl), 298.1 K.

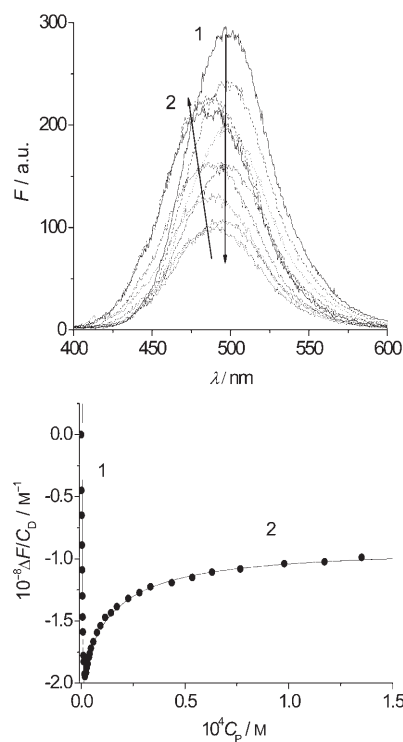
D (phase 1) followed by an intensity increase (phase 2) and a shift of the emission maximum towards smaller wavelengths (Figure 3, top). Figure 3 (bottom) shows the fluorescence titration performed at $I = 0.11$ M, pH 7, $\lambda_{\text{exc}} = 385$ nm, $\lambda_{\text{em}} = 500$ nm and $T = 298.1$ K. The binding isotherm evidences the biphasic behaviour of the system, and reveals the occurrence of two different modes of interaction.

The interaction of DNA with the Zn^{II} complex of **D** has been investigated as well. The measurements were performed at pH 8 at which the complex $[\text{ZnD}]^{2+}$ is practically the only species in solution. The high stability constant of this species (Table 1) ensures that the complex is completely formed prior to reaction with DNA and that the metal ion is retained by **D**, thus the spectral changes observed after mixing the preformed complex with a solution of CT-DNA only reflect the occurrence of a polymer–dye binding reaction.

The spectral behaviour of the $[\text{ZnD}]$ –DNA system (Supporting Information, Figure S4) is similar to that of the **D**–DNA system and the features of the binding isotherms evidence biphasic behaviour for this system as well.

From now on, we shall indicate the first branch of the titration curve (decrease of fluorescence) as binding mode 1 and the second branch of the curve (enhancement of fluorescence) as binding mode 2.

The binding process can be represented by the apparent reaction given in Equation (1) in which the dye (**D**) interacts with the DNA (**P**) to give the bound species (**PD**). The equilibrium constant of this reaction is defined as $K = [\text{PD}] / ([\text{P}] \times [\text{D}])$.

Figure 3. Spectrofluorimetric analysis of the binding of **D** to DNA; $C_{\text{D}} = 1 \times 10^{-6}$ M, C_{P} in the range $0 - 1.75 \times 10^{-4}$ M, $I = 0.11$ M (NaCl), pH 7, 298.1 K, $\lambda_{\text{exc}} = 385$ nm. Top: Fluorescence spectra collected during titration; the spectral changes reveal the biphasic behaviour of the binding process. Bottom: Binding isotherm recorded at $\lambda_{\text{em}} = 500$ nm; the two phases, 1 and 2, are associated to two different binding modes.

To evaluate the binding parameters of the two binding modes, the two branches of the titration curves were analysed according to Equation (2), in which C_{D} and C_{P} are the total dye and polymer concentrations respectively; $\Delta F = F - \varphi_{\text{D}} C_{\text{D}}$ is the change of fluorescence (F) during titration; $\varphi_{\text{D}} = F^{\circ} / C_{\text{D}}$, in which F° denotes the initial fluorescence of

the dye solution and $\Delta\varphi = \varphi_{PD} - \varphi_D$ is the amplitude.

$$\Delta F/C_D = (K\Delta\varphi \times C_p)/(1+KC_p) \quad (2)$$

The analysis of the branches of the titration curves allows us to evaluate K and $\Delta\varphi$ for the two binding modes (K_1 , $\Delta\varphi_1$ and K_2 , $\Delta\varphi_2$ respectively). The values of K_1 and K_2 are collected in Table 2. The quality of the fit is shown in Figure 3 (bottom), for which the continuous line is calculated by using Equation (2).

Table 2. Reaction parameters for the interaction of CT-DNA with **D** and [Zn**D**], 298.1 K.

Dye	I [M]	$10^{-6} K_1$ [M ⁻¹]	$10^{-4} K_2$ [M ⁻¹]
D	0.01	1.7	24
	0.11	1.3	6.9
	1.0	0.41	< 1.0
[Zn D]	0.01	6.9	20
	0.11	5.7	5.6
	1.0	4.3	3.7
proflavine	0.10	–	6.6 ^[31]
	0.20	–	2.0 ^[32]
	0.24	–	4.3 ^[33] (283 K)

Salt effect: Fluorescence titrations have been carried out at different salt concentrations. Because **D** and [Zn**D**] are positively charged ($[H_3D]^{3+}$, $[ZnD]^{2+}$) under the experimental conditions adopted for DNA binding, a salt dependence of the equilibria is likely to occur. In effect, the binding isotherms of the **D**–DNA system show a dependence on ionic strength going from $I=0.01$ M to $I=1.01$ M (NaCl). At $I=0.01$ M and $I=0.11$ M the biphasic nature of the binding process is evident, whereas at $I=1.01$ M a monophasic behaviour is observed (Figure 4, top).

Two modes of binding are also present at $I=1.01$ M (Figure 4, bottom) for the [Zn**D**]–DNA system; this reveals that the metal ion plays a role in the interaction of the zinc complex with DNA. Table 2 summarises the results.

Dye displacement assay: To better understand the nature of the binding process, a fluorescent intercalator displacement assay^[34] was applied to the **D**–DNA and [Zn**D**]–DNA systems by adding CT-DNA, which had been previously saturated with the intercalating cyanine dye (Cyan40), to samples of **D** or [Zn**D**]. The cyanine dye strongly interacts with DNA by intercalation, and in doing so hinders the penetration of further agents between base pairs. Moreover, its emission spectrum does not overlap with those of **D** and [Zn**D**]. The titrations show that binding mode 1 is still present, while the binding mode 2 is strongly reduced (Figure 5).

Table 3 reports the values of the ratio $\Delta\varphi_2/\Delta\varphi_1$ between the amplitudes of binding mode 2 and binding mode 1 in the absence and in the presence of the cyanine. For the **D**–DNA system, the amplitude ratio in the presence of cyanine is ten-times smaller than that found with DNA alone, whereas

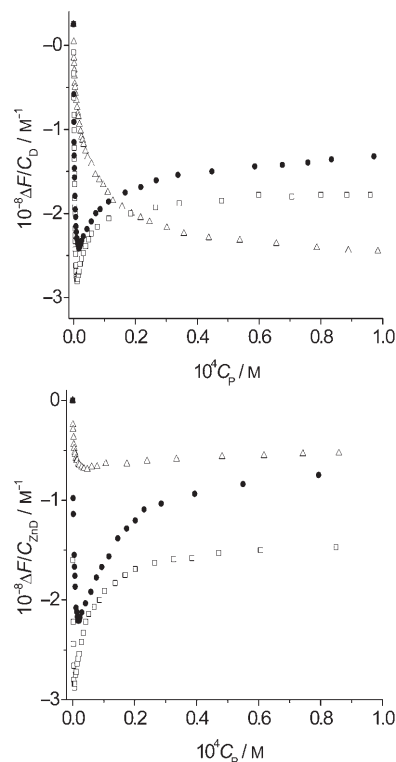


Figure 4. Top: Binding isotherms in fluorescence detection for the **D**–DNA system at different ionic strengths. □: $I=0.01$ M; ●: $I=0.11$ M; △: $I=1.01$ M. $\lambda_{em}=500$ nm, pH 7.0, 298.1 K. Bottom: Binding isotherms in fluorescence detection for the [Zn**D**]–DNA system at different ionic strengths. □: $I=0.01$ M; ●: $I=0.11$ M; △: $I=1.01$ M. $\lambda_{em}=500$ nm, pH 8.0, 298.1 K. $C_D = C_{[ZnD]} = 1 \times 10^{-6}$ M.

for the [Zn**D**]–DNA system this ratio is about four-times smaller.

Absorbance measurements: Absorbance titrations confirm the biphasic behaviour described above. Absorbance spectra of the **D**–DNA system were recorded during titrations, and showed that the absorbance first decreases (phase 1, which corresponds to binding mode 1) and then increases (phase 2, which corresponds to binding mode 2) and displays a bathochromic shift (Supporting Information, Figure S5 A). A similar feature is exhibited by the [Zn**D**]–DNA system (Supporting Information, Figure S5 B).

Circular dichroism measurements: The CD spectra of **D**–DNA and [Zn**D**]–DNA have been recorded under conditions for which binding mode 2 is prevalent. Also the CD spectrum of the proflavine–DNA system has been recorded for comparison (Figure 6). The CD spectra of **D**–DNA (Figure 6a) and [Zn**D**]–DNA (Figure 6b) are quite similar, and their shapes resemble that of proflavine intercalated into DNA (Figure 6c) in that the positive band appears at longer wavelengths with respect to the negative one.^[35] The shifts of spectra a) and b), with respect to c), along the wavelength axis depends on the position of the absorption band of proflavine, which is less energetic than the absorption bands of

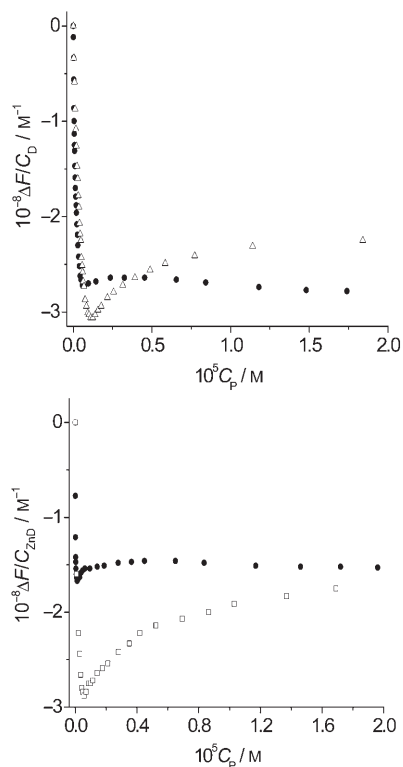


Figure 5. Top: Fluorescence titration of **D** in the presence of DNA (Δ) and DNA previously saturated with Cyan40 (\bullet). $I=0.01$ M, pH 7.0, 298.1 K and $\lambda_{em}=500$ nm. Bottom: Fluorescence titration of [**ZnD**] in presence of DNA (Δ) and DNA previously saturated with Cyan40 (\bullet). $I=0.01$ M, pH 8.0, 298.1 K and $\lambda_{em}=500$ nm. $C_D=C_{[ZnD]}=1 \times 10^{-6}$ M.

Table 3. The ratio between the amplitude of the binding mode 2 and the binding mode 1 in a traditional titration, $\Delta\varphi_2/\Delta\varphi_1$, and in presence of DNA saturated with Cyan40, $(\Delta\varphi_2/\Delta\varphi_1)_{Cyan40}$. $\lambda_{em}=500$ nm, 298.1 K.

	$\Delta\varphi_2/\Delta\varphi_1$	$(\Delta\varphi_2/\Delta\varphi_1)_{Cyan40}$
D –DNA	–0.34	–0.029
[ZnD]–DNA	–0.50	–0.13

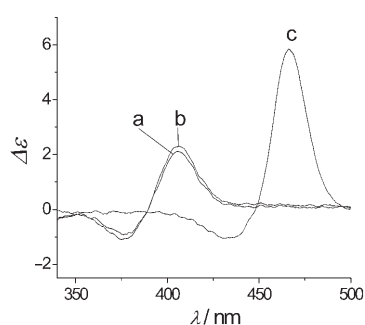


Figure 6. Circular dichroism spectra of a) **D**–DNA, b) [**ZnD**]–DNA and c) proflavine–DNA systems. $C_D=3.0 \times 10^{-5}$ M, $C_P=3.0 \times 10^{-5}$ M, pH 7.0, $I=0.11$ M (NaCl) and 298.1 K.

D and [**ZnD**]. Similarly, the higher amplitude of the proflavine band can be ascribed to the higher absorptivity of this dye. This finding is in agreement with the intercalative features of binding mode 2.

Unwinding measurements: To obtain further information on the DNA-binding mode, an unwinding assay was performed. Incubation of supercoiled DNA with topoisomerase I gives rise to relaxed DNA, and upon removal of the protein the relaxed state is maintained. In contrast, when an intercalating agent is present in the reaction mixture it alters the topological state of circular-closed DNA, and upon removal of both dye and enzyme, supercoiled DNA is suddenly re-generated. The magnitude of superhelicity is determined by the original amount of bound dye and the unwinding angle at the time of the enzymatic religation.^[36] An example of a supercoiled-DNA unwinding experiment is reported in Figure 7. The presence of a supercoiled plasmid is clearly

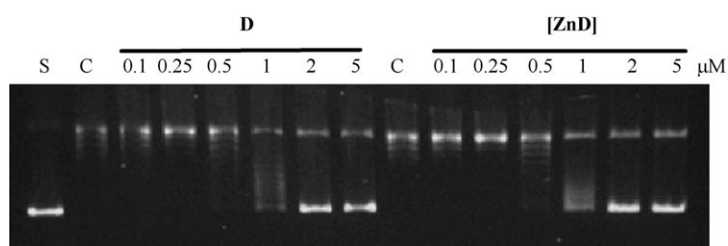


Figure 7. Topoisomerase I relaxation reactions of supercoiled pBR322 DNA performed in the presence of increasing concentrations of **D** and [**ZnD**]. S refers to supercoiled pBR322 DNA; C refers to relaxed pBR322 DNA obtained by incubating the plasmid DNA with the enzyme in the absence of dye.

evidenced starting from $1 \mu\text{M}$ of **D** or [**ZnD**]; this confirms their ability to bind DNA through an intercalation mode. It is interesting to note that **D** and [**ZnD**] showed comparable efficiency in altering the enzyme-induced relaxation of the supercoiled plasmid; this suggests comparable stability of the intercalated complexes.

Kinetics: The kinetics of the interaction between **D** and DNA were investigated in a range of dye and polymer concentrations at which binding mode 2 is operative. Relaxation times (τ) were measured under pseudo-first-order conditions ($C_P \geq 10C_D$) and kinetic traces were fitted by mono-exponential functions (Supporting Information, Figure S6). A plot of the reciprocal time constant ($1/\tau$) as a function of DNA concentration (C_P) shows that the kinetic effect is independent of the polynucleotide concentration (Figure 8, top).

The [**ZnD**]–DNA system has been studied under analogous conditions. The analysis of the data reveals that also in this case the kinetics are independent of the DNA concentration (Figure 8, bottom).

Molecular modelling: The conformational analysis of the ligand molecule was carried out before the in silico investigation of its binding mode to the biological target. In particular the attention was focused on the $[\text{H}_3\text{D}]^{3+}$ species, which is predominant in aqueous solution at the pH value (pH 7) that was used for the binding studies.

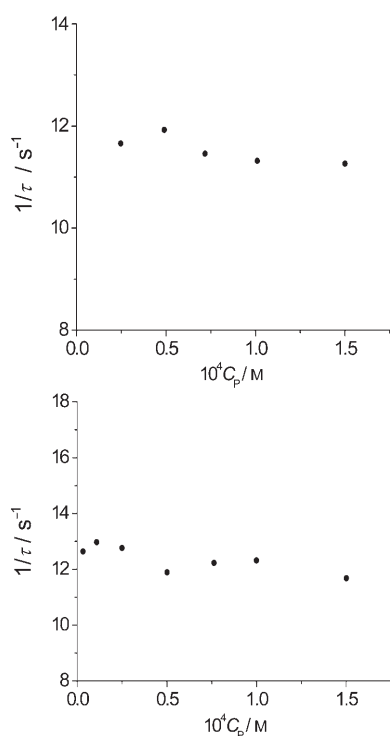


Figure 8. Top: Dependence of the reciprocal relaxation time, $1/\tau$, on the polynucleotide concentration for the **D**-DNA system. $I=0.11$ M (NaCl), 298.1 K, pH 7.0, $\lambda_{\text{ex}}=405$ nm (laser). Bottom: Dependence of the reciprocal relaxation time, $1/\tau$, on the polynucleotide concentration for the **[ZnD]**-DNA system. $I=0.11$ M (NaCl), 298.1 K, pH 8.0, $\lambda_{\text{ex}}=405$ nm (laser). $C_{\text{D}}=C_{[\text{ZnD}]}=4 \times 10^{-6}$ M.

Analysis of the structural parameters of acridine molecules that had been functionalised with $C_{\text{ar}}\text{-NH-}C_{\text{al}}$ groups (C_{ar} and C_{al} stand for aromatic and aliphatic C atoms, respectively) linked to the C9 position was carried out with the ConQuest^[37] and VISTA programs^[38] on the Cambridge Structural Database.^[39] This showed mainly sp^2 character for this type of nitrogen atom, although a partial loss of conjugation between the nitrogen atom and the aromatic moiety was commonly found. The most frequent value for the $C_{\text{ar}}\text{-}C_{\text{ar}}\text{-NH-}C_{\text{al}}$ dihedral angle is about 20° , which is usually correlated with a $C_{\text{ar}}\text{-NH-}C_{\text{al}}$ bond angle ranging from $125\text{--}135^\circ$.

As a consequence, a Nsp^2 atom type was assigned to this nitrogen atom, and both dihedral and angular values were constrained to the above-mentioned values.

Three conformers (Supporting Information), each from one of the most populated clusters, were selected to study the binding of $[\text{H}_3\text{D}]^{3+}$ to the biological target. All the conformers had antiperiplanar torsional angles of the C_6 chain (*trans* conformation) and mainly differed from each other in the orientation of the diethylentriamine moiety with respect to the acridine plane, which was almost perpendicular in two of them, and almost coplanar in the third one.

The modelling study of the interaction between the ligand and the selected DNA decamers (see Experimental Section) was carried out by considering both the intercalative and

non-intercalative binding modes and by investigating the interaction of the ligand with both the minor and major grooves of DNA. Moreover, a set of five characteristic basis sequences that featured 60% CG and 40% AT base-pair composition, analogous to that of CT-DNA, was considered.

By taking into account the different DNA sequences and the different interacting modes, several docking experiments of the three $[\text{H}_3\text{D}]^{3+}$ conformers were planned and performed. Appropriate experimental settings and conditions were used to avoid effects on the docking results due to ligand interaction with the polymer ends. Furthermore, both CG and AT sites were considered for the intercalative binding mode. The ΔE energies for the different poses, namely the predicted adduct structures, which actually give rise to favourable interaction (Supporting Information, Table S1) were calculated according to Equation (3).

$$\Delta E = E_{\text{adduct}} - \sum E_{\text{reagent}} \quad (3)$$

Inspection of the ΔE values clearly evidences that the main binding mode for the considered **P/D** ratio should be intercalation. However, two different intercalative modes should be available, *parallel* and *perpendicular*, when the proflavine group intercalates in a parallel or perpendicular fashion to the base-pair hydrogen bonds.^[40] In the parallel mode the intercalator interacts with both DNA filaments, while in the perpendicular mode only one filament is mostly involved in the π -stacking interaction.

The two intercalative binding modes are depicted in Figure 9, which shows adducts obtained with the GCGCGCGCGC (left) and CGCGATATCG (right) sequences. Selected structural information (Table S2) and figures (Figure S7) for all calculated adducts are reported in Supporting Information.

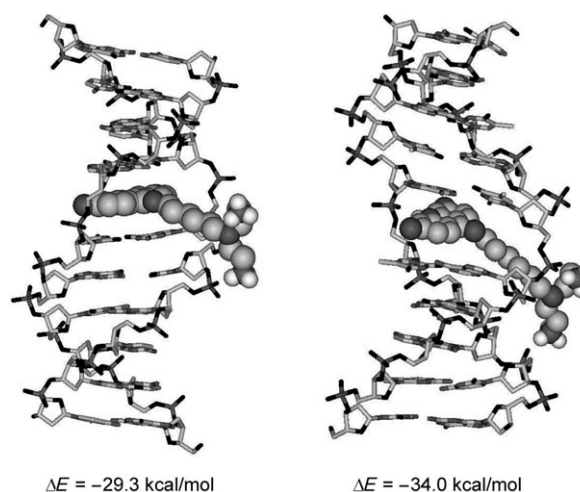
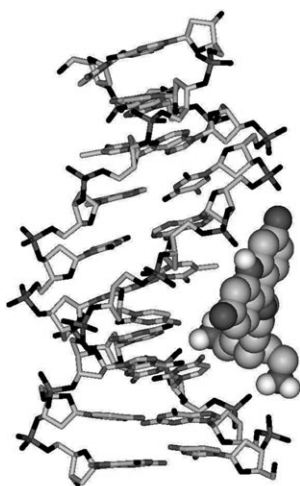


Figure 9. Adducts obtained with GCGCGCGCGC (left) and CGCGATATCG (right) sequences showing parallel and perpendicular intercalative binding modes, respectively. ΔE values are calculated interaction energies.

It should be noted that in the perpendicular binding mode, hydrogen-bond and electrostatic interactions are often present that involve the protonated acridine nitrogen and oxygen atoms of the polymer. On the other hand, the polyamine chain, which is accommodated in the major or in the minor groove of the different adducts, contributes to the overall stability through the formation of one or two hydrogen-bond contacts with the phosphate groups.

Several adducts that are derived from nonintercalative binding were also predicted by the molecular-modelling calculations. As an example, Figure 10 shows the adduct that



$$\Delta E = -19.05 \text{ kcal/mol}$$

Figure 10. Adduct obtained with the CGCGATATCG sequence featured by major-groove-binding mode. ΔE is calculated interaction energy.

was obtained for the CGCGATATCG sequence (Supporting Information, Tables S1 and S2) in which the protonated ligand lies in the major groove. The adduct is stabilised by hydrogen-bond interactions with the phosphate oxygen of the polyanion that involved both protonated acridine and aliphatic nitrogens, and by a $\text{CH}\cdots\pi$ interaction between a T base and the acridine ligand moiety ($\text{CH}_3\cdots\text{C}$ mean distance = 3.9 Å).

Discussion

Self-aggregation of acridine orange,^[23] proflavine and other similar dyes^[24] was shown to produce modifications of the electronic absorption spectra of the monomeric species that were interpreted by assuming the formation of dimers in solutions at low concentration, as the principal species in equilibrium with the monomeric forms. Accordingly, it seems reasonable that the unique oligomeric species that is formed by **D** under our experimental conditions is a dimer, which is in agreement with the ^1H NMR spectroscopy data. Unfortunately, in the case of **D**, absorption spectra cannot be used

to analyse the nature of the aggregate, because, as shown by ^1H NMR measurements, the formation of this species takes place at concentrations greater than $1 \times 10^{-3} \text{ M}$ of **D**; this concentration range corresponds to absorbance values that are not suitable for binding studies. In the case of the Zn^{II} complex, although similar problems were found in the analysis of self-aggregation by means of absorption spectra, potentiometric measurements make it possible to establish the dimeric nature of the aggregates and determine their formation constants (Table 1).

The analysis of the ^1H NMR spectra of the aggregates furnishes some indications about the relative orientation of the adjacent molecules in these aggregates. In the case of the metal-free ligand, the acridine protons and the proton of the hydrogen atom H4, which is linked to the carbon atom in the proximity of the acridine group, are subjected to the shielding effect of the aromatic π -clouds, as denoted by the significant upfield shift of the corresponding ^1H NMR resonances (Figure 1). The two signals that shift the most are those of H1 and H4 ($\delta_{\text{H1}} - \delta_{\text{H1}'} = 0.096 \text{ ppm}$, $\delta_{\text{H4}} - \delta_{\text{H4}'} = 0.126 \text{ ppm}$, Figure 1), which indicates that these two hydrogen atoms penetrate more deeply into the shielding region of the aromatic groups with respect to H2 and H3 ($\delta_{\text{H2}} - \delta_{\text{H2}'} = 0.046 \text{ ppm}$, $\delta_{\text{H3}} - \delta_{\text{H3}'} = 0.042 \text{ ppm}$, Figure 1). A possible arrangement of the aggregate that would account for the observed ^1H NMR behaviour is depicted in Figure 11. This shows a **D** dimer in which two face-to-face

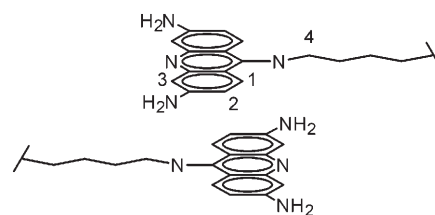


Figure 11. Proposed arrangement of **D** dimers.

π -stacked molecules, disposed in a head-to-tail mode, have the centres of the adjacent aromatic rings laterally displaced towards H1 and H4. Such an arrangement would cause the chelating hanging groups to be located in the deshielding zone of the aromatic systems, which is in agreement with the downfield shift that is experienced by the relevant ^1H NMR signals in the aggregate with respect to the monomeric molecule (Figure 1). Similar considerations can be made for the Zn^{II} complex of **D**, the aggregation mode of which is probably quite similar to that of the metal-free ligand.

Analogous interaction modes were also reported for proflavine,^[41] acridine orange^[21,42] and acridine orange derivatives.^[26,43]

This study has shown that the bifunctional molecule **D** and its Zn^{II} complex ($[\text{ZnD}]$) interact with double-stranded DNA, to form stable complexes. Static measurements clear-

ly show a biphasic behaviour for both systems, which reveals the occurrence of two different modes of binding.

The decrease of fluorescence emission and absorbance signals, observed for the first branch of titrations (binding mode 1), persists varying the ionic strength. The values of K_1 related to this mode of binding are two orders of magnitude higher than those expected for intercalation reactions in spite of the fact that the approximation made in Equation (2) ($[P] = C_p$) would cause K_1 to be underestimated.

One can note that the values of K_1 for both **D**-DNA and **[ZnD]**-DNA systems display a slight ionic-strength dependence, possibly due to charge effects.^[44] The major difference between the two systems lies in the fact that the affinity of **[ZnD]** for DNA is near four times greater than that of **D**; this suggests that, in binding mode 1, the residue that contains the zinc ion plays an important role.

The enhancement of fluorescence emission and the observed red shift of the absorbance spectra during the second part of the titrations (binding mode 2) indicate a base-dye interaction. The values of the related binding constant, K_2 , are close to the value that was measured for the DNA-proflavine system (Table 2), which is known to bind double-stranded nucleic acids by intercalation.^[31-33] Because **D** and **[ZnD]** bear +3 and +2 charges ($[H_3D]^{3+}$, $[ZnD]^{2+}$), respectively, the slopes of $\log K$ versus $-\log [Na^+]$ plots could be much higher ($\cong 3$ and $\cong 2$). The lower values that were obtained suggest that not the entire molecule, but only the proflavine residue takes part in binding mode 2. Actually, the charge of this residue is +1 for **D** and smaller than 1 for **[ZnD]**. For these reasons we suggest that binding mode 2 corresponds to the intercalation of the aromatic residue into DNA, whereas the first part of titration (binding mode 1) is related to the formation of an external complex between the dye and DNA.

The dye displacement assay shows for both systems that upon the addition of DNA saturated with an intercalating dye, the first binding stage still remains whereas the second one is suppressed (Figure 5). This behaviour indicates that **D** is not able to push the intercalated dye out of the nucleotide cavities, otherwise a fluorescence increase would be observed at the wavelength of 500 nm at which only the **D**-DNA complex, which is formed according to binding mode 2, is fluorescent. Because it is demonstrated that Cyan40 is intercalated between the base pairs of DNA,^[45] the binding mode 2 necessarily should correspond to an intercalative process. This hypothesis was confirmed by the unwinding assay as well as by CD experiments. Similar considerations can be applied to the **[ZnD]**-DNA system.

The observation that the first branch of the titration curves is not influenced by the presence of cyanine intercalated into DNA suggests that in binding mode 1 the interaction between the dye and DNA occurs externally to the DNA cavities, with the polyamine residue possibly lying along the grooves of the nucleic acids. The calculated model depicted in Figure 10 could provide a general idea of this type of non-intercalative interaction, although it is not representative of the specific structural features of **D**-DNA ad-

ducts formed under the conditions of binding mode 1 (low dye-to-DNA molar ratios).

The kinetics of **D** and **[ZnD]**-binding to DNA according to binding mode 2 show that the values of the time constants of the two systems are similar; this suggests that the rate-determining step involves a residue common to both dyes, that is, the proflavine residue. This is in agreement with the comparable binding constant that is observed in the presence/absence of the metal ion for the second equilibrium, which gives rise to comparable efficiency in DNA unwinding. The values of the rate constants are an order of magnitude lower than the value expected for diffusion-controlled reactions,^[46] this fact confirms that the binding process, which is represented by the apparent reaction (1), is not a simple one, but is composed of at least two steps.

The kinetic features of binding mode 2 could be rationalised on the basis of the reaction Equation (4), in which **P**-**D** is a bound form that is different from the intercalate **PD_{int}**. According to Equation (4) the kinetic data could be fitted to Equation (5)



$$1/\tau = (K_{ex}k_1C_p)/(1 + K_{ex}C_p) + k_{-1} \quad (5)$$

If $K_{ex}C_p \gg 1$, it turns out that $1/\tau = (k_1 + k_{-1})$ and its concentration dependence could not be observed.

Structural information on the adducts that were formed with DNA were obtained by means of modelling studies that were performed with DNA sequences (decamers), which are representative of the calf thymus DNA base-pair composition. A 1:1 decamer/**D** molar ratio was adopted that corresponds to the range of concentration at which the binding mode 2 was observed. By taking into account the similar behaviour of **D** and **[ZnD]** in DNA-binding mode 2, only modelling studies based on **D** were performed.

The proton localisation that was determined for $[H_3D]^{3+}$ by means of ¹H NMR measurements in solution (Scheme 1) was used in both a preliminary conformational search and in docking procedures, by assuming that no changes occur upon interaction with DNA.

As previously reported, the nitrogen atom of the $C_{ar}-NH-C_{al}$ linkage has mostly a sp^2 character, and therefore it should have neither hydrogen-bond acceptor properties nor donor ability towards metal ions. Actually, similar binding processes are found in both **D**-DNA and **ZnD**-DNA systems, in agreement with the fact that the $C_{ar}-NH-C_{al}$ group is not involved in metal coordination.

The analysis of modelling results (see Supporting Information, Tables S1 and S2) shows that intercalation is the preferred binding mode, in agreement with the solution results obtained for the binding mode 2 with calf thymus DNA and with literature data on other acridine-type compounds.^[47] Intercalative binding involves both AT and CG base pairs, even if CG sequences seem to be preferred to AT ones. Most likely, in the case of the polyA-polyT sequence, major-groove binding should occur also.

Inspection of the geometrical features of the calculated adducts reveals that both parallel and perpendicular stacking modes (Figure 9) should occur in the **D**-DNA system, the perpendicular one is favoured by additional $\text{NH}^+\cdots\text{O}$ interactions between the protonated acridine nitrogen atom and the oxygen atoms of the polyanion.

The perpendicular stacking with acridine-type compounds is rather surprising, because they are usually reported as parallel base-stacking intercalators.^[47] For instance, the acridine-type drug 9-amino-DACA, which interacts with DNA in its protonated form, behaves as a parallel bis-intercalator.^[48] However, it is worth noting that in the case of 9-amino-DACA an intramolecular hydrogen bond that involves the protonated heteroaromatic nitrogen of the drug avoids the formation of hydrogen-bond and/or salt-bridge interactions with the biological target. This is not the case of $[\text{H}_3\text{D}]^{3+}$, which forms additional $\text{NH}^+\cdots\text{O}$ interactions in several **D**-DNA species, which enhance the stability of perpendicular adducts.

Nevertheless, the perpendicular intercalation mode has been proposed for several intercalators such as doxorubicin and daunomycin^[49] as well as for acridines^[50,51] for which it was denoted as a half-intercalation. According to this model, the dye intercalates between two adjacent bases of one of the two strands, while the positive charge interacts electrostatically with the phosphate groups of the DNA backbone.^[52,53]

Conclusion

The new proflavine-based ligand that contains a hanging chelating diethylenetriamine moiety and its Zn^{II} complex bind to calf thymus DNA according to a biphasic behaviour that is defined by two different binding modes depending on the polymer-to-dye molar ratio (**P/D**); the ligand forms complexes of considerable stability. At relatively low **P/D** values, both the metal-free ligand and its Zn^{II} complex associate with DNA externally to the base pairs; the principal involvement comes from the polyamine moiety. The presence of the metal ion leads to a fourfold increase of the dye affinity for the polymer. On the other hand, at high **P/D** values the interaction takes place through intercalation of the proflavine residue between base pairs; significant effects are not derived from the presence of Zn^{II} .

Molecular-modelling calculations were performed with appropriate base pair sequences and showed that the intercalative binding should be more favourable when the CG base pairs are involved, even if intercalation between AT base pairs also leads to stable complexes. Most likely, in the case of the AT sequence, significant groove binding also occurs.

In contrast with the common behaviour of base-stacking intercalators, modelling calculations indicate that the intercalative binding of the present dye should mostly involve only one filament of the double helix (Figure 9, right), probably due to $\text{NH}^+\cdots\text{O}$ interactions between the protonated

acridine nitrogen and the oxygen atoms of the polyanion. Most likely this peculiar binding feature is favoured by the structure of the intercalator, which was designed with the intention of inserting the chelating hanging group onto the C9 atom of acridine in order to allow the N10 atom to project towards the polymer chain.

These results may help in the design of new intercalators in support of improved DNA-binding processes.

Experimental Section

General details: Stock solutions of **D** (2×10^{-3} M) were prepared by dissolving weighed amounts of the solid in pure DMSO, and were kept in the dark at 255 K. Working solutions were obtained by diluting the stocks to such a level that the DMSO content could be neglected, and were used shortly after preparation. A solid sample of Cyan40^[54] was provided by Prof. S. Yarmoluk and the relevant stock solution was prepared as described for **D**.

Calf thymus DNA was purchased from Pharmacia Biotech (Uppsala, Sweden), in the form of the lyophilised sodium salt, dissolved into water and sonicated as described below. Stock solutions were standardised spectrophotometrically, by using $\epsilon = 13200 \text{ mol}^{-1} \text{ dm}^3 \text{ cm}^{-1}$ at 260 nm, $I = 0.1 \text{ M}$ (NaCl), pH 7 as obtained from the sample certificate. The polynucleotide concentrations are expressed in molarity of base pairs and are indicated as C_p . Sodium chloride was used to adjust the ionic strength, and sodium cacodylate (1×10^{-2} M) was employed to keep the pH of the solutions to the desired value.

The **D**-DNA system was studied at pH 7.0 and the **[ZnD]**-DNA system at pH 8.0. All solutions were prepared with double-distilled water, which was also used as the reaction medium.

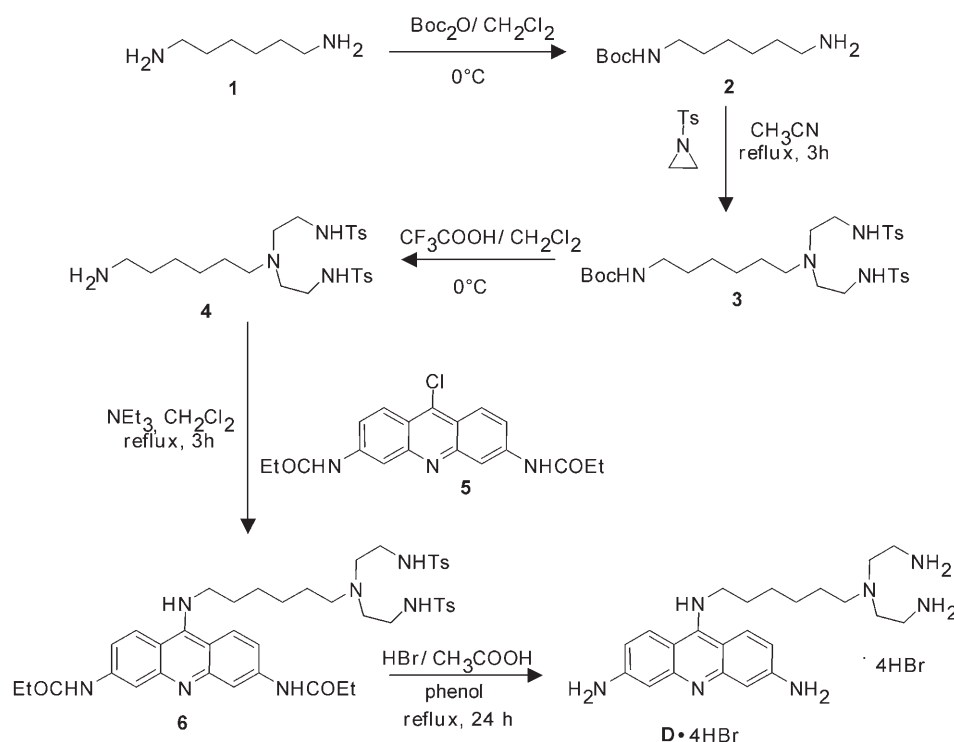
DNA sonication was carried out by using an MSE-Soniprep sonicator (Sanyo Gallenkamp, Leicestershire, UK), by applying seven repeated cycles of 10 s sonication and 20 s pause to a DNA sample (10 mL of CT-DNA $\approx 2 \times 10^{-3}$ M), at an amplitude of 14 μm . The sonicator tip was introduced directly into the solution; this solution was kept in an ice bath to minimise thermal effects due to sonication. Agarose gel electrophoresis tests indicated that the polymer length was reduced to about 800 base-pairs.

^1H and ^{13}C NMR spectra were recorded at 298 K on a Varian Unity 300 MHz instrument. In ^1H NMR spectra peak positions are reported relative to HOD at $\delta = 4.75$ ppm (D_2O) or to TMS (CD_3OD , CDCl_3), while in ^{13}C spectra peak positions are reported relative to 1,4-dioxane at $\delta = 67.2$ ppm (D_2O) or TMS (CD_3OD , CDCl_3). In the pH-metric titrations, small amounts of 0.01 M NaOD or DCl were added to adjust the pD. The pH was calculated from the measured pD value by using the relationship $\text{pH} = \text{pD} - 0.40$.^[55]

ESI mass spectra were performed with a ESI Mass TSO 700 FINNINGAM by using the free ligand **D**, which was obtained by extraction in chloroform of an aqueous alkaline solution prepared from **D**·4HBr·EtOH.

Synthesis of ligand (N^9 -[6-[bis(2-aminoethyl)amino]hexyl]-acridine-3,6,9-triamine) (D**):** Ligand **D** was obtained as a hydrobromide salt (**D**·4HBr), according to the reaction sequence shown in Scheme 2. Compound **5** was prepared by a reported method.^[56]

Synthesis of tert-butyl (6-aminoethyl)carbamate (2**):** Boc₂O (31.6 g, 0.145 mol) was added in small portions to a solution of 1,6-diaminohexane (50.5 g, 0.43 mol) in CH_2Cl_2 (350 mL) at 0 °C (water/ice bath). The mixture was maintained overnight at room temperature, then chloroform (375 mL) was added and the resulting solution was washed twice with a 5% Na_2CO_3 aqueous solution (750 mL). The organic phase was dried over anhydrous Na_2SO_4 and the solvent was removed under reduced pressure to obtain a sticky residue, which was dissolved in 1 M HCl solution (50 mL) and washed three times with diethyl ether (50 mL). The resulting aqueous solution was alkalised by the addition of 2 M NaOH



Scheme 2. Reaction sequence for the synthesis of **D**.

(13 mL) and the compound was extracted with ethyl acetate (5 × 200 mL). The organic solution was successively dried over anhydrous Na₂SO₄ and vacuum evaporated to obtain a solid compound, which was further dried under vacuum at room temperature in the presence of KOH. Yield 11.6 g (37%); ¹H NMR (CDCl₃): δ = 1.38 (s, 9H), 1.42–1.50 (m, 8H), 2.32 (s, 2H), 2.65 (m, 2H), 3.04 (m, 2H), 4.67 ppm (s, 1H); ¹³C (CDCl₃): δ = 26.4, 26.5, 28.4, 30.0, 33.3, 40.4, 41.9, 78.9, 155.9 ppm; elemental analysis calcd (%) for C₁₁H₂₄N₂O₂: C 61.08, H 11.18, N 12.95; found: C 61.02, H 11.23, N 12.89.

Synthesis of tert-butyl[6-bis[2-[[4-(4-methylphenyl)sulfonyl]amino]ethyl]amino]hexyl]carbamate (3): A solution of *N*-tosyl aziridine (11.0 g, 0.056 mol) in dry acetonitrile (140 mL) was added to a refluxing solution of **2** (5.0 g, 0.023 mol) in dry acetonitrile (140 mL) over a period of 3 h. The solution was refluxed for further 3 h, then the solvent was removed under reduced pressure to obtain a pale-yellow oil, which was successively subjected to chromatography on silica gel (CH₂Cl₂/MeOH 100:3) mixture. The eluted fractions were combined and evaporated to dryness under reduced pressure. Yield: 7.35 g, 85%; ¹H NMR (CDCl₃): δ = 1.09 (m, 2H), 1.20 (m, 4H), 1.39 (m, 2H), 1.42 (s, 9H), 2.17 (m, 2H), 2.40 (s, 6H), 2.42 (m, 4H), 2.86 (m, 4H), 3.04 (m, 2H), 4.63 (s, 1H), 5.61 (s, 2H), 7.28 (d, *J* = 8.0 Hz, 4H), 7.76 ppm (d, *J* = 8.0 Hz, 4H); ¹³C (CDCl₃): δ = 21.6, 26.0, 26.5, 26.9, 28.5, 29.9, 40.6, 53.1, 53.4, 79.0, 127.0, 129.6, 136.7, 143.1, 155.8 ppm; elemental analysis calcd (%) for C₂₉H₄₆N₄O₆S₂: C 57.02, H 7.59, N 9.17; found: C 57.07, H 7.53, N 9.24.

Synthesis of *N,N'*-[[6-aminohexyl]imino]diethane-2,1-diyl]bis(4-methylbenzenesulfonamide) (4): CF₃COOH (150 mL) was added dropwise to a solution of **3** (7.35 g, 0.012 mol) in CH₂Cl₂ (120 mL) at 0°C (water/ice bath). The resulting solution was maintained at room temperature for 24 h, then cooled in a water/ice bath and alkalised by the addition of 2 M NaOH (660 mL). The organic phase was separated, and the aqueous phase was extracted with CH₂Cl₂ (3 × 200 mL). The organic solutions were combined and dried over anhydrous Na₂SO₄. The solvent was then eliminated by evaporation under reduced pressure to obtain compound **4**, as a sticky yellow oil, in quantitative yield. ¹H NMR (CDCl₃): δ = 1.02–1.34 (m, 6H), 1.39 (m, 2H), 2.18 (m, 2H), 2.38 (m, 4H), 2.40 (s, 6H), 2.68 (m, 2H), 2.86 (m, 4H), 3.86 (s, 4H), 7.29 (d, *J* = 8.0 Hz, 4H),

7.76 ppm (d, *J* = 8.0 Hz, 4H); ¹³C (CDCl₃): δ = 21.6, 26.1, 26.2, 26.6, 40.6, 41.5, 53.0, 127.0, 129.6, 136.7, 143.0 ppm; elemental analysis calcd (%) for C₂₄H₃₈N₄O₄S₂: C 56.44, H 7.50, N 10.97; found: C 56.50, H 7.41, N 11.04.

Synthesis of *N,N'*-[9-[[6-bis[2-[[4-(4-methylphenyl)sulfonyl]amino]ethyl]amino]hexyl]amino]acridine-3,6-diyl]dipropanamide (6): A suspension of **4** (1.64 g, 3.2 mmol), **5** (*N,N'*-[9-chloroacridine-3,6-diyl]dipropanamide) (1.14 g, 0.0032 mol) and NEt₃ (0.45 mL, 0.0032 mol) in dry acetonitrile (50 mL) was refluxed for 5 h.

The solvent was then removed under reduced pressure and the dark-orange crude compound was subjected to chromatography on silica gel (CH₂Cl₂/MeOH 100:15) mixture. The eluted fractions were combined and evaporated under reduced pressure. The resulting solid orange compound was further dried in vacuum at room temperature. Yield: 2.15 g, 81%; ¹H NMR (CD₃OD): δ = 1.23 (t, *J* = 7.6 Hz, 6H), 1.28–1.40 (m, 4H), 1.44 (m, 2H), 1.92 (m, 2H), 2.32 (t, *J* = 6.2 Hz, 2H), 2.38 (s, 6H), 2.44 (t, *J* = 6.3 Hz, 4H), 2.49 (q, *J* = 7.6 Hz, 4H), 2.82 (t, *J* = 6.3 Hz, 4H), 4.01 (t, *J* = 7.3 Hz, 2H), 7.31 (d, *J* = 8.1 Hz, 4H), 7.35 (dd, *J* = 9.2,

2.1 Hz, 2H), 7.68 (d, *J* = 8.1 Hz, 4H), 8.26 (d, *J* = 9.2 Hz, 2H), 8.27 ppm (d, *J* = 2.1 Hz, 2H); ¹³C NMR (CD₃OD): δ = 9.8, 21.5, 27.5, 27.6, 27.8, 30.7, 31.3, 42.0, 50.1, 54.7, 55.0, 106.1, 109.7, 117.5, 127.5, 128.0, 130.7, 138.6, 142.8, 144.6, 145.7, 156.9, 176.0 ppm; elemental analysis calcd (%) for C₄₅H₅₅N₇O₆S₂: C 62.22, H 6.68, N 11.81; found: C 62.11, H 6.71, N 11.76.

Synthesis of *D*•4HBr•EtOH: A solution containing **6** (1.90 g, 0.0023 mol) and phenol (10.8 g, 0.11 mol) in 33% HBr/CH₃COOH (370 mL) was maintained at 90°C under stirring for 24 h. The resulting suspension was then cooled to room temperature and CH₂Cl₂ (350 mL) was added to complete the precipitation of the light-orange compound, which was filtered, washed with CH₂Cl₂, recrystallised from an EtOH/H₂O (3:1 v/v) mixture and dried in vacuum at 308 K in the presence of KOH to obtain **D**•4HBr•EtOH. Yield 0.80 g, 45%; ¹H NMR (D₂O, pH 3.8): δ = 1.12–1.68 (m, 8H), 2.52 (m, 2H), 2.80 (m, 4H), 3.11 (m, 4H), 3.19 (m, 2H), 5.96 (d, *J* = 2.2 Hz, 2H), 6.45 (dd, *J* = 9.5, 2.2 Hz, 2H), 7.28 ppm (d, *J* = 9.5 Hz, 2H); ¹³C NMR (D₂O, pH 3.8): δ = 25.2, 26.7, 26.9, 30.1, 37.5, 48.8, 50.8, 52.8, 97.1, 104.3, 114.3, 141.3, 153.0 ppm; MS: *m/z*: 410.36 [M+H]⁺; UV/Vis (H₂O, pH 2.1, 298 K): λ_{max} (ε) = 383 (25500), 275 nm (50200 mol⁻¹ dm³ cm⁻¹); elemental analysis calcd (%) for C₂₅H₃₅N₇Br₄O: C 38.53, H 5.82, N 12.58, Br 45.06; found: C 38.61, H 5.77, N 12.73, Br 44.95 (the bromide content was evaluated by potentiometric titrations of the compound with AgNO₃).

Potentiometric measurements: All pH-metric measurements (pH = -log[H⁺]) that were employed for the determination of equilibrium constants were carried out in 0.1 M NMe₄Cl solutions at 298.1 ± 0.1 K, by using equipment and methodology already described.^[57] The combined Hamilton glass electrode (LIQ-GLASS 238000/08) was calibrated as a hydrogen concentration probe by titrating known amounts of HCl with CO₂-free NaOH solutions and by determining the equivalent point by Gran's method^[58] which allows one to determine the standard potential, *E*⁰, and the ionic product of water (p*K*_w = 13.83(1) at 298.1 K in 0.1 M NMe₄Cl). At least three measurements were performed for each system in the pH ranges 2.5–10.5. In ligand protonation experiments, the concentration of ligand C_D was 5 × 10⁻⁴ M. In complexation experiments the con-

centration of **D** was varied in the range 1×10^{-4} – 1×10^{-3} M, while the concentration of Zn^{II} was $C_D \leq C_{ZnII} \leq 2C_D$. The computer program HYPER-QUAD^[59] was used to calculate the equilibrium constants from the electromotive force data.

Spectral measurements: Absorption spectra were recorded on a Perkin-Elmer Lambda 35 spectrophotometer and fluorescence emission spectra on a Perkin-Elmer LS 55 spectrofluorimeter at 298.1 ± 0.1 K. The titration experiments for ligand protonation and Zn^{II} -complexation studies were performed in 0.1 M NMe₄Cl solution. Spectrophotometric titrations of the dye alone and its Zn^{II} complex with calf thymus DNA were carried out at $I = 0.11$ M (NaCl) and $\lambda = 390$ nm, by adding increasing amounts of DNA solution directly into the cell containing the dye ($C_D = 1 \times 10^{-5}$ M) or its Zn^{II} -complex solution ($C_{[ZnD]} = 1 \times 10^{-5}$ M).

Fluorescence titrations of DNA samples were performed at $\lambda_{exc} = 385$ nm and $\lambda_{em} = 480$ or 500 nm by using the procedure above described.

Circular dichroism spectra were recorded on a Jasco J710 spectropolarimeter (Easton, MD, USA).

Kinetic measurements: The kinetic measurements were carried out on a Biologic SFM 300 stopped-flow mixing unit coupled to a spectrophotometric line by two optical guides. A blue laser diode ($\lambda = 405$ nm, 1 mW) was used as a light source. The radiation was passed through a Bausch and Lomb 338875 high-intensity monochromator and then split into two beams. The reference beam was sent directly to a 1P28 photomultiplier. The measuring beam was sent through an optical quartz guide to the observation chamber and then, through a second optical guide, to the measuring photomultiplier, which was also IP28. The output from the two photomultipliers was balanced before each shot. The stopped-flow apparatus is able to measure absorbance and/or fluorescence changes, but only the fluorescence detection mode was employed. The acquisition system keeps a record of a number of data points ranging from 10–8000 with sampling intervals ranging from 50 μ s–10 s. Each experiment was repeated at least ten times, and the relaxation curves obtained were averaged by an accumulation procedure. All measurements were carried out under pseudo-first-order conditions.

Unwinding measurements: Supercoiled pBR322 DNA (0.15 μ g) was incubated with 1 U of topoisomerase I (Invitrogen) in Tris HCl (50 mM), pH 7.5, KCl (50 mM), MgCl₂ (10 mM), DTT (0.5 mM), EDTA (100 μ M), BSA (30 μ g mL⁻¹) in the presence/absence of increasing concentrations of **D** or [ZnD]. After overnight incubation at 310 K, NaCl was added to the samples to a final concentration of 0.15 M and, the samples were extracted with an equal volume of 1:1 PhOH/CHCl₃ that was buffered to pH 7.5 with Tris HCl (50 mM), to eliminate both the dye and protein. The aqueous phase was loaded on 1% agarose gel, and run in TAE (40 mM Tris, 18 mM acetic acid, 1 mM EDTA). The reaction products were visualised by ethidium bromide staining.

Molecular modelling: Computations were performed on AMD 1 GHz and Intel P4 3 GHz computers running Linux.

The conformational search was performed by using the simulated annealing (SA) procedure contained in MacroModel version 8.5,^[60] by using the MMFF force field (FF) and the atomic partial charges from FF. The settings of the molecular dynamic simulation were as follow: running temperature: $T = 400$ K; heating, running and cooling time: 5 ps; time step: 1.5 fs. 100 Energy-minimised conformers were obtained and collected in cluster by using an "in house"-developed routine that was written in Visual Basic programming language version 6.0 (Microsoft Corporation). The routine groups molecules on the basis of the root mean square (RMS) value of the distance between atoms ($RMS \leq 0.9$ Å).

DNA decamers in the B-form were built by using the Builder module in Maestro version 7.5^[61] for all the following sequences: ATATATATAT, GCGCGCGCGC, ATCGCGCGAT, CGCGATATCG, CGATCGATCG. Intercalation sites of CG and/or AT types were conveniently built in the centre of the decamers for each DNA sequence.

Docking calculations were performed by using the Glide program.^[62] Default input parameters were used in all computations (no scaling factor for the vdW radii of nonpolar DNA atoms, 0.8 scaling factor for nonpolar ligand atoms). The grids for the docking (20 Å edges for the enclosing box) were centred on the centroid of the appropriate residues, and were

chosen according to the intercalative and non-intercalative binding modes.

Upon completion of each docking calculation, twenty poses per ligand were saved. The overall sixty conformers that were obtained for H₃D³⁺ were clustered on the basis of the position that was assumed with respect to the DNA double helix and were ranked according to the glide score. The top-ranked conformer per cluster was selected. The DNA–ligand complexes were submitted to a minimisation with Impact v.4.0,^[63] OPLS2005 force-field-based conjugate gradient minimisation routine (atomic charges from the FF, maximum number of minimisation cycle: 5000; energy change criterion: 0.01 kcal mol⁻¹ Å⁻¹; gradient criterion: 0.01). Continuum representation of the solvent have been used by means of the Poisson–Boltzmann solver equation.^[64]

Acknowledgement

The authors wish to thank Prof. S. Yarmoluk for the kind gift of a Cyan40 sample.

- [1] S. Neidle, *Prog. Med. Chem.* **1979**, *16*, 151–221.
- [2] H. M. Berman, P. R. Yuong, *Annu. Rev. Biophys. Bioeng.* **1981**, *10*, 87–114.
- [3] W. P. Wilson, R. L. Jones, *Adv. Pharmacol. Chemother.* **1981**, *18*, 177–222.
- [4] R. Zittoun, *Eur. J. Cancer Clin. Oncol.* **1985**, *21*, 649–653.
- [5] A. Albert, *The Acridines: Their Preparation, Physical, Chemical, and Biological Properties and Uses*, Arnold, London, **1966**.
- [6] L. S. Lerman, *J. Mol. Biol.* **1961**, *3*, 18–30.
- [7] A. Aggarwal, S. A. Islam, R. Kuroda, S. Needle, *Biopolymers* **1984**, *23*, 1025–1041.
- [8] A. Adams, *Curr. Med. Chem.* **2002**, *9*, 1667–1675.
- [9] L. Malinina, M. M. Soler-López, J. Aymami, J. A. Subirana, *Biochemistry* **2002**, *41*, 9341–9348.
- [10] L. P. G. Wakelin, M. J. Waring, *J. Mol. Biol.* **1980**, *144*, 183–214.
- [11] S. Lippard, *Acc. Chem. Res.* **1978**, *11*, 211–217.
- [12] C. Hiort, P. Lincoln, B. Norden, *J. Am. Chem. Soc.* **1993**, *115*, 3448–3454.
- [13] S. Arounagui, D. Easwaramoorthy, A. Ashokkumar, A. Dattagupta, G. M. Bhaskar, *Proc. Indian Acad. Sci. Chem. Sci.* **2000**, *112*, 1–17.
- [14] A. H. Krotz, B. P. Hudson, J. K. Barton, *J. Am. Chem. Soc.* **1993**, *115*, 12577–12578; R. H. Terbrueggen, J. K. Barton, *Biochemistry* **1995**, *34*, 8227–8234.
- [15] K. E. Erkkila, D. T. Odom, J. K. Barton, *Chem. Rev.* **1999**, *99*, 2777–2795.
- [16] E. J. C. Olson, D. Hu, A. Hoermann, A. M. Jonkman, M. R. Arkin, E. D. A Stemp, J. K. Barton, P. F. Barbara, *J. Am. Chem. Soc.* **1997**, *119*, 11458–11467.
- [17] A. C. Lim, J. K. Barton, *Bioorg. Med. Chem.* **1997**, *5*, 1131–1136.
- [18] B. A. Jackson, J. K. Barton, *J. Am. Chem. Soc.* **1997**, *119*, 12986–12987; B. A. Jackson, V. Y. Alekseyev, J. K. Barton, *Biochemistry* **1999**, *38*, 4655–4662.
- [19] L. G. Marzilli, S. Ano, F. P. Intini, G. Natile, *J. Am. Chem. Soc.* **1999**, *121*, 9133–9142.
- [20] E. A. Boudreaux, *Int. J. Quantum Chem.* **2001**, *83*, 255–258.
- [21] B. E. Bowler, K. J. Ahmed, W. I. Sundquist, L. S. Hollis, E. E. Whang, S. J. Lippard, *J. Am. Chem. Soc.* **1989**, *111*, 1299–1306.
- [22] C. Ciatto, M. L. D'Amico, G. Natile, F. Secco, M. Venturini, *Bio-phys. J.* **1999**, *77*, 2717–2724.
- [23] M. E. Lamm, D. M. Neville, Jr., *J. Phys. Chem.* **1965**, *69*, 3872–3877.
- [24] R. W. Chambers, T. Kajiwara, D. R. Kearns, *J. Phys. Chem.* **1974**, *78*, 380–387.
- [25] H. Porumb, *Prog. Biophys. Mol. Biol.* **1978**, *34*, 175–195.
- [26] D. J. Blears, S. S. Danyluk, *J. Am. Chem. Soc.* **1967**, *89*, 21–26.
- [27] R. Luchowski, S. Krawczyk, *Chem. Phys.* **2003**, *293*, 155–166.
- [28] A. N. Glazer, *Proc. Natl. Acad. Sci. USA* **1965**, *54*, 171–176.

- [29] R. M. Smith, A. E. Martell, NIST Stability Constants Database, version 4.0, National Institute of Standards and Technology, Washington, DC, **1997**.
- [30] B. Adcock, in *Acridines*, 2nd ed. (Ed.: R. M. Acheson) Interscience, New York, **1973**, pp. 109–137.
- [31] T. Biver, F. Secco, M. R. Tinè, M. Venturini, *Arch. Biochem. Biophys.* **2003**, *418*, 63–70.
- [32] H. J. Li, D. M. Crothers, *J. Mol. Biol.* **1969**, *39*, 461–477.
- [33] M. Dourlent, J. F. Hogrel, *Biochemistry* **1976**, *15*, 430–436.
- [34] a) W. C. Tse, D. L. Boger, *Acc. Chem. Res.* **2004**, *37*, 61–69; b) T. Biver, D. Lombardi, F. Secco, M. R. Tinè, M. Venturini, A. Bencini, A. Bianchi, B. Valtancoli, *Dalton Trans.* **2006**, *10*, 1524–1533; c) T. C. Jenkins, *Methods in Molecular Biology*, Humana Press, Totowa, **1997**, pp. 195–218.
- [35] D. G. Dalglish, H. Fujita, A. R. Peacocke, *Biopolymers*, **1969**, *8*, 633–645.
- [36] S. M. Zeman, K. M. Depew, S. J. Danishefsky, D. M. Crothers, *Proc. Natl. Acad. Sci. USA* **1998**, *95*, 4327–4332.
- [37] ConQuest Version 1.8, Cambridge Crystallographic Data Centre, 12 Union Road CB 1EZ, UK.
- [38] VISTA version 2.1, Cambridge Crystallographic Data Centre, 12 Union Road CB 1EZ, UK.
- [39] a) CSD version 5.27 (November 2005); b) F. H. Allen, J. E. Davies, J. J. Galloy, O. Johnson, O. Kennard, C. F. Macrae, E. M. Mitchell, G. F. Mitchell, J. M. Smith, D. G. Watson, *J. Chem. Inf. Comput. Sci.* **1991**, *31*, 187–204.
- [40] J. N. Lisgarten, M. Coll, J. Portugal, C. W. Wright, J. Aymami, *Nat. Struct. Biol.* **2002**, *9*, 57–60.
- [41] a) S. Neidle, T. A. Jones, *Nature* **1975**, *253*, 284–285; b) S. K. Obendorf, H. L. Carrell, J. P. Glusker, *Acta Crystallogr. Sect. B* **1974**, *30*, 1408–1411.
- [42] a) E. R. Gordon, R. B. Walsh, W. T. Pennington, T. W. Hanks, *J. Chem. Crystallogr.* **2003**, *33*, 385–390; b) C. A. Mattia, L. Mazzarella, V. Vitagliano, R. Puliti, *J. Crystallogr. Spectrosc. Res.* **1984**, *14*, 71–87.
- [43] a) R. Puliti, C. A. Mattia, L. Mazzarella, *Acta Crystallogr., Sect. C* **2002**, *58*, 582–584; b) R. Puliti, C. A. Mattia, *Acta Crystallogr. Sect. A* **2001**, *57*, 1338–1340.
- [44] H. Li, X. Peng, P. Leonard, F. Seela, *Bioorg. Med. Chem.* **2006**, *14*, 4089–4100.
- [45] T. Biver, A. De Biasi, F. Secco, M. Venturini, S. Yarmoluk, *Biophys. J.* **2005**, *89*, 374–383.
- [46] H. Strehlow, *Rapid Reaction in Solution*, Wiley-VCH, Weinheim, **1992**, p. 16.
- [47] H. Baruah, U. Bierbach, *Nucleic Acids Res.* **2003**, *31*, 4138–4146.
- [48] A. Adams, J. M. Guss, C. A. Collyer, W. A. Denny, L. P. G. Wakelin, *Biochemistry* **1999**, *38*, 9221–9223.
- [49] C. A. Frederick, L. D. Williams, G. Ughetto, G. A. Van der Marel, J. H. Van Boom, A. Rich, A. H. J. Wang, *Biochemistry* **1990**, *29*, 2538–2549.
- [50] N. J. Pritchard, A. Blake, A. R. Peacocke, *Nature* **1966**, *212*, 1360–1361.
- [51] A. Blake, A. R. Peacocke, *Biopolymers*, **1968**, *6*, 1225–1253.
- [52] “Techniques and Applications of Fast Reactions in Solution”: T. Yanusaga, H. Ushio, in *NATO ASI Ser. Ser. C* **1979**, *50*, 389–397.
- [53] M. Kamiya, *Biochim. Biophys. Acta* **1978**, *517*, 527–530.
- [54] S. S. Lukashov, M. Y. Losytsky, Y. L. Slominskii, S. M. Yarmoluk, *Biopolym. Cell.* **2001**, *17*, 169–177.
- [55] A. K. Covington, M. Paabo, R. A. Robinson, R. G. Bates, *Anal. Chem.* **1968**, *40*, 700–706.
- [56] S. A. Gamage, N. Tepsiri, P. Wilairat, S. J. Wojcik, D. P. Figgitt, R. K. Ralph, W. A. Denny, *J. Med. Chem.* **1994**, *37*, 1486–1494.
- [57] A. Bianchi, L. Bologni, P. Dapporto, M. Micheloni, P. Paoletti, *Inorg. Chem.* **1984**, *23*, 1201–1205.
- [58] a) G. Gran, *Analyst (London)* **1952**, *77*, 661–671; b) F. J. Rossotti, H. Rossotti, *J. Chem. Educ.* **1965**, *42*, 375–378.
- [59] P. Gans, A. Sabatini, A. Vacca, *Talanta* **1996**, *43*, 1739–1753.
- [60] a) F. Mohamadi, N. G. J. Richards, W. C. Guida, R. Liskamp, M. Lipton, C. Caufield, G. Chang, T. Hendrickson, W. C. Still, *J. Comput. Chem.* **1990**, *11*, 440–467; b) L. L. C. Schrödinger, New York <http://www.schrodinger.com>.
- [61] Maestro v 7.5, L. L. C. Schrödinger, New York <http://www.schrodinger.com>.
- [62] a) R. A. Friesner, J. L. Banks, R. B. Murphy, T. A. Halgren, J. Klicic, D. T. Mainz, M. P. Repasky, E. H. Knoll, M. Shelley, J. K. Perry, D. E. Shaw, P. Francis, P. S. Shenkin, *J. Med. Chem.* **2004**, *47*, 1739–1749; b) L. L. C. Schrödinger, New York <http://www.schrodinger.com>.
- [63] Impact v 4.0, L. L. C. Schrödinger, New York <http://www.schrodinger.com>.
- [64] M. C. Cortis, R. A. Friesner, *J. Comput. Chem.* **1997**, *18*, 1591–1608.

Received: December 21, 2006

Revised: June 13, 2007

Published online: September 13, 2007